THE JOURNAL OF BIOLOGICAL CHEMISTRY
Vol. 279, No. 33, Issue of August 13, pp. 34913–34921, 2004
Printed in U.S.A.

The Topography of Transmembrane Segment Six Is Altered during the Catalytic Cycle of P-glycoprotein*

Received for publication, May 13, 2004, and in revised form, June 9, 2004
Published, JBC Papers in Press, June 10, 2004, DOI 10.1074/jbc.M405336200

Alice Rothnie‡§, Janet Storm‡, Jeff Campbell¶, Kenneth J. Linton‖, Ian D. Kerr, and Richard Callaghan‡ ‡‡**

*From the ‡Nuffield Department of Clinical Laboratory Sciences, John Radcliffe Hospital, University of Oxford, Oxford, OX3 9DU, ¶Laboratory of Molecular Biophysics, University of Oxford, Rex Richards Bldg., South Parks Rd., Oxford OX1 3QU, ‖Medical Research Council Clinical Sciences Centre, Imperial College School of Medicine, Hammersmith Hospital Campus, Du Cane Rd., London, W12 0NN, and **Centre for Biochemistry and Cell Biology, School of Biomedical Sciences, University of Nottingham, Queen's Medical Centre, Nottingham, NG7 2UH, United Kingdom*

Structural evidence has demonstrated that P-glycoprotein (P-gp) undergoes considerable conformational changes during catalysis, and these alterations are important in drug interaction. Knowledge of which regions in P-gp undergo conformational alterations will provide vital information to elucidate the locations of drug binding sites and the mechanism of coupling. A number of investigations have implicated transmembrane segment six (TM6) in drug-P-gp interactions, and a cysteine-scanning mutagenesis approach was directed to this segment. Introduction of cysteine residues into TM6 did not disturb basal or drug-stimulated ATPase activity *per se*. Under basal conditions the hydrophobic probe coumarin maleimide readily labeled all introduced cysteine residues, whereas the hydrophilic fluorescein maleimide only labeled residue Cys-343. The amphiphilic BODIPY-maleimide displayed a more complex labeling profile. The extent of labeling with coumarin maleimide did not vary during the catalytic cycle, whereas fluorescein maleimide labeling of F343C was lost after nucleotide binding or hydrolysis. BODIPY-maleimide labeling was markedly altered during the catalytic cycle and indicated that the adenosine 5′-(β,γ-imino)triphosphate-bound and ADP/vanadate-trapped intermediates were conformationally distinct. Our data are reconciled with a recent atomic scale model of P-gp and are consistent with a tilting of TM6 in response to nucleotide binding and ATP hydrolysis.

The ubiquitously expressed P-glycoprotein (P-gp,[1] ABCB1) is a "multidrug" transporter capable of mediating the translocation of numerous chemically and functionally unrelated compounds. The broad selectivity is based on the presence of multiple drug binding sites (1–4) that are localized within the transmembrane domains (TMDs) (5, 6). P-gp is a primary active transporter belonging to the ATP binding cassette family (7), and ATP hydrolysis occurs in the two cytosolic nucleotide binding domains (NBDs) (8), both of which are essential for transport activity (9, 10). Active transport mechanisms require (i) binding site re-orientation and (ii) binding site affinity changes that are directly coupled to the provision of energy, usually through ATP hydrolysis (11, 12). These fundamental events in a transport cycle have been demonstrated for P-gp, and the data have generated possible models outlining the sequence of binding site changes driven by nucleotide binding and hydrolysis (13, 14).

The mechanism of coupling the drug binding event to ATP hydrolysis is, however, poorly understood for P-gp. Drug binding to the TMDs is known to stimulate ATP hydrolysis (15, 16) and modulate the fluorescence characteristics of a probe attached within the NBD (17), providing evidence for TMD → NBD communication. The reverse communication pathway has also been observed (18), and numerous biophysical techniques have demonstrated that P-gp undergoes tertiary structural changes in response to both nucleotide binding and subsequent hydrolysis (19, 20). Direct evidence that the TMDs undergo functionally important conformational transitions has been obtained from structural investigations using electron microscopy of two-dimensional crystals (21, 22). However, this evidence does not indicate which of the 12 transmembrane segments is affected or which protein regions transduce the communication between TMDs and NBDs.

Structural evidence has proposed that the TMD is organized into a "ring" of protein surrounding a central aqueous pore (21, 22) similar to the arrangement of the TMDs observed in the atomic resolution structures for the bacterial ABC transporters BtuCD (23) and MsbA (24). Initial topographical maps using cysteine-scanning mutagenesis rejected the symmetric and mirror image arrangements of TM segments for P-gp in favor of the "cyclone model" (25). However, a more recent manuscript by the same authors has revised this model (26), reverting to the initial suggestion of a ring of helices surrounding the aqueous central pore. Clearly, more work is required to elucidate the precise configuration of TM segments in P-gp. A consistent feature of such investigations has been that (i) TM segments 6 and 12 approach each other at the cytoplasmic membrane face (25, 27, 28), and (ii) the TM segments 5, 6, 11, and 12 are in close proximity (25, 29). Recently, an atomic scale model of P-gp, based on the MsbA structure, has been proposed that agrees with the two points taken from cross-linking data (30). This model allows more focused site-directed mutagenesis investigations to fully elucidate the protein topography.

The earliest attempts to elucidate the drug binding site(s)

* This work was funded by Cancer Research United Kingdom Program Grant SP1861/0401. The costs of publication of this article were defrayed in part by the payment of page charges. This article must therefore be hereby marked "*advertisement*" in accordance with 18 U.S.C. Section 1734 solely to indicate this fact.

§ Recipient of a Medical Research Council Ph.D. studentship.
‡‡ To whom correspondence should be addressed: Tel.: 44-1865-221-110; Fax: 44-1865-221-834; E-mail: richard.callaghan@ndcls.ox.ac.uk.

[1] The abbreviations used are: P-gp, P-glycoprotein; ABC, ATP binding cassette family; TM6, transmembrane (TM) segment 6; NBD, nucleotide binding domain; ANOVA, one-way analysis of variance; CM, 7-diethylamino-3-(4′-maleimidylphenyl)-4-methylcoumarin; FM, fluorescein-5-maleimide; BM, 4,4-difluoro-1,3,5,7-tetramethyl-8-(4-maleimidylphenyl)-4-bora-3a,4a-diaza-*s*-indacene; AMP-PNP adenosine 5′-(β,γ-imino)triphosphate.

labeled P-gp with photoactivable drugs and identification of proteolytic fragments using specific antibodies (5, 6, 31, 32). The labeled fragments comprised elements of TM helices 5, 6, 11, and 12, although many other species were observed. A recent investigation using the more sophisticated mass spectroscopic approach identified similar structural elements (33). However, it is worth noting that a major drawback with photoactivable drugs is their inherent reactivity and, thus, may label residues distant to the actual pharmacophoric region (34). Investigations employing mutagenesis approaches identified numerous residues throughout the TM segments of P-gp that contribute to protein function (35–38). They were not confined to a single TM segment; however, a significant proportion was localized to TM6. Selection of cell lines in actinomycin D (39) or doxorubicin with PSC833 (40) produced expression of P-gp with mutations to different residues within TM6, and in both cases the mutation led to an altered spectrum of resistance compared with wild type protein. Site-directed mutagenesis also indicated that residues Ser-337, Val-338, Ile-340, Gly-341, Ala-342, Ser-344, and Gly-346 were involved in drug transport by P-gp. Because most of these investigations use cellular drug resistance profiles as the indicator for P-gp function. it is unclear what aspect of the transport cycle was impaired (*e.g.* drug binding or allosteric communication). These lines of circumstantial evidence clearly implicate TM6 as playing a defining role in the overall transport mechanism. TM6 is directly linked to the N-terminal NBD, and a role in communication may be hypothesized.

The present investigation uses a cysteine-scanning mutagenesis approach combined with fluorescent labeling to elucidate the topography of this key TM segment in P-gp. The protein was then trapped in nucleotide-bound and post-hydrolytic conformations of the catalytic cycle to ascertain the nature of conformational changes in TM6 produced by events in the NBDs. The results were explained using the recently described atomic model of P-gp.

EXPERIMENTAL PROCEDURES

Materials—BODIPY-maleimide, fluorescein-maleimide, and coumarin-maleimide were all purchased from Molecular Probes (Leiden, NL). Octyl-β-D-glucoside and nickel nitrilotriacetic acid His Bind Superflow resin were obtained from Merck. [^{3}H]Phosphatidylcholine (83 Ci/mmol) was purchased from Amersham Biosciences, and dimethyl sulfoxide (Me_2SO) disodium adenosine triphosphate (Na_2ATP), cholesterol, vinblastine, nicardipine and sodium orthovanadate were all from Sigma. Crude *Escherichia coli* lipid extract was obtained from Avanti Polar Lipids (Alabaster, AL). Insect-Xpress medium was purchased from Cambrex BioScience (Nottingham, UK), and Excell 405 was from AMS Biotechnology (Abingdon, UK). All other reagents were of at least analytical grade.

Production of Recombinant Baculovirus—Expression and characterization of a cysteine-less, histidine-tagged P-gp in mammalian cells has been described (41, 42). Single cysteines were introduced into the cysteine-less multidrug resistance (MDR1)-coding sequence by site-directed mutagenesis as described previously (41). The following mutagenic oligonucleotides were used (5′ to 3′; in each case the cysteine codon is in bold): oligoV331C, TCTATTGGACAA**TGC**CTCACTGTA; oligoT333C, ATTGGACAAGTTCTC**TG**CGTATTCTTTTC; oligoF335C, CTCACTGTATGCTTTTCTGTGTTAATTGGG; oligoS337C, CTGTATTCTTTTG**TGT**GTTAATTGGG; oligoL339C, CTTTTCTGTA**TGC**ATTGGGGCT; oligoG341C, CTGTATTAATT**TGC**GCATTTAGTGTTGG; oligoF343C, TTTTCTGTATTGATTGGGGCT**TGT**AGTGTTGG.

Additionally, all oligonucleotides were designed to generate a restriction site, which is silent with respect to the coding sequence. This was done to monitor subsequent cloning steps by restriction digest profiles (italicized if outside the cysteine codon). The nucleotide sequences of the mutated DNA fragments were verified by DNA sequencing. The entire coding sequence for cysteine-less-P-gp and single cysteine mutants, including the 5′ Kozak sequence, was introduced into the baculoviral transfer vector pBacPAK9 (Clontech), and recombinant baculoviruses were generated by *in vivo* recombination with BacPAK6 DNA (Clontech).

Expression of P-gp and Isolation of Insect Cell Membranes—The *Trichoplusia ni* (High Five) cell line was routinely used for the expression of P-gp and maintained in shaking suspension cultures as previously described (42). High Five cells at a density of ~3.10^6 cells/ml were infected with recombinant baculovirus (~5.10^7 plaque-forming units/ml) at a multiplicity of infection of 5. After 2 h of incubation with virus, the cells were diluted to a density of 1.5×10^6 cells/ml and grown for a further 3 days before harvesting by centrifugation ($2000 \times g$ for 10 min). Crude membrane preparations were isolated as previously described (42), and the final membrane preparations were stored in high sucrose buffer at −80 °C for up to 6 months before further use.

Purification and Reconstitution of P-gp—Membrane preparations were solubilized in buffer containing 2% (w/v) octyl-β-D-glucoside and P-gp-purified using nickel nitrilotriacetic acid by virtue of the C-terminal hexahistidine tag. Reconstitution of the purified protein was achieved by selective detergent adsorption, and efficiency was monitored by comparing lipid and protein migration after sucrose density gradient ultracentrifugation. Full details of the purification and reconstitution procedures have been described previously (42, 43).

Determination of Protein Concentration—Commercial protein assay kits could not be used to quantify P-gp concentrations due to unacceptable levels of interference due to the presence of lipids, imidazole, and glycerol. Consequently, a densitometric analysis of Coomassie-stained SDS-PAGE gels was used. The P-gp bands were compared with a series of known amounts of bovine serum albumin (0.2–1.0 μg) on the same gel. Gels were stained with 0.25% (w/v) Coomassie Blue (1–2 h) in 50% (v/v) methanol and 10% (v/v) acetic acid. Destaining was achieved using 5% (v/v) methanol in 10% (v/v) acetic acid. The intensity of protein bands was determined by quantitative densitometry using the NIH Image Software.

Measurement of ATP Hydrolysis—ATP hydrolysis was determined by measurement of inorganic phosphate liberation using a colorimetric assay (44) with previously described modifications (42). Reconstituted protein (0.3 μg) was incubated at 37 °C for 20 min with varying concentrations of Na_2ATP (0–1.75 mM). To determine the drug-stimulated ATPase activity, samples were incubated with 30 μM nicardipine. The ATPase activity (nmol of P_i released/min/mg of P-gp) was plotted as a function of ATP concentration, and the maximal velocity (V_{max}) and substrate affinity (K_mATP) were determined by non-linear regression of the Michaelis-Menten equation.

Where information on the effects of drugs on P-gp activity was required, the ATPase activity was measured as above except at a constant ATP concentration of 2 mM. The drugs (nicardipine and vinblastine) were added from stocks in Me_2SO to provide a range between 10^{-9} and 10^{-4} M. The ATPase activity was plotted as a function of drug concentration, and the potency of effect (EC_{50} or IC_{50}) was derived from non-linear regression of the general dose-response equation,

$$V = V_{min} + \frac{V_{max} - V_{min}}{1 + 10^{(\log EC_{50} - [L])}} \quad \text{(Eq. 1)}$$

where V is the rate of ATP hydrolysis, V_{min} is minimal activity, V_{max} is maximal activity, and [L] is drug concentration.

Octanol:Water Partition Coefficient—The polarities of the three fluorescent probes, coumarin-maleimide (CM), fluorescein-maleimide (FM), and BODIPY-maleimide (BM) were determined by assessment of relative partitioning between aqueous and octanol solutions. Fluorophores were added to 1 ml of buffer (20 mM Tris-HCl, pH 6.8) in a concentration range of 3–100 μM. Octanol (1 ml) was added, and the solutions were mixed by rotation for at least 12 h at 20 °C to reach partition equilibrium. After phase separation, absorption spectra were recorded (Hitachi U-1200 spectrophotometer), and the maximal absorbance was determined according to Beer's Law. The extinction coefficients were: FM = 83,000 cm^{-1} M^{-1}, CM = 33,000 cm^{-1} M^{-1}, and BM = 88,000 cm^{-1} M^{-1} as provided by the manufacturer (Molecular Probes, Leiden NL). The ratio of the amount in the octanol compared with the aqueous phase was calculated (P). The $\log_{10}$ of this ratio (log P) indicates the relative polarity.

Time Courses for Labeling of Single Cysteine-containing P-gp Isoforms—The time courses for reaction of maleimide-containing probes with single cysteine mutant P-gp isoforms were undertaken to enable determination of both the extent of labeling and the half-life describing the reaction. Purified, reconstituted P-gp (1.5–3 μg) was incubated at 20 °C with fluorescent probes (10 μM) for 0, 10, 20, 30, 60, 120, 180, and 300 min. These conditions provided at least a 100-fold molar excess of probe to P-gp to ensure that ligand depletion did not occur. Probes were added from concentrated stocks in Me_2SO, and the final solvent concentration did not exceed 0.5% (v/v). Reaction with probe was termi-

TABLE I

Characteristics of basal and drug-stimulated ATPase activity for purified reconstituted single cysteine mutants of P-gp

Pure, reconstituted P-gp (0.3 μg) was incubated in the presence of varying ATP concentrations (0–1.75 mM), and the ATPase activity was determined by measurement of inorganic phosphate liberation. Basal activity was measured in the absence of any drugs, whereas stimulated activity was determined in the presence of 30 μM nicardipine. The substrate affinity (K_m) and maximal activity (V_{max}) were determined by non-linear regression of the Michaelis-Menten equation. -Fold stimulation was determined by the ratio of V_{max} (stimulated)/V_{max} (basal). Values refer to the mean ± S.E. obtained from at least eight independent protein purification preparations.

P-gp isoform	Substrate affinity , K_m		Maximal activity, V_{max}		-Fold stimulation
	Basal	Stimulated	Basal	Stimulated	
	mM		*μmol P_i min^{-1} mg protein^{-1}*		
Cys-less	0.58 ± 0.06	0.38 ± 0.04	0.58 ± 0.15	1.46 ± 0.30	2.9 ± 0.3
V331C	0.50 ± 0.06	0.26 ± 0.02	0.45 ± 0.05	1.54 ± 0.20	3.5 ± 0.3
T333C	0.49 ± 0.05	0.23 ± 0.02	0.35 ± 0.04	1.22 ± 0.15	3.3 ± 0.1
F335C	0.40 ± 0.05	0.24 ± 0.03	0.65 ± 0.15	1.61 ± 0.31	2.2 ± 0.2
S337C	0.53 ± 0.06	0.26 ± 0.04	0.59 ± 0.10	1.67 ± 0.23	3.2 ± 0.4
L339C	0.51 ± 0.07	0.31 ± 0.04	0.57 ± 0.07	1.47 ± 0.15	2.9 ± 0.3
G341C	0.40 ± 0.04	0.24 ± 0.02	0.42 ± 0.03	1.12 ± 0.09	3.1 ± 0.5
F343C	0.41 ± 0.04	0.26 ± 0.03	0.47 ± 0.04	1.17 ± 0.15	2.6 ± 0.3

nated by the addition of excess dithiothreitol (100 μM), and the samples were immediately placed on ice. Samples were diluted 1:1 in buffer (20 mM Tris-HCl, pH 7.4, 150 mM NH_4Cl, 5 mM $MgSO_4$, 0.02% NaN_3) to reduce the glycerol content and subjected to ultracentrifugation (125,000 × *g*, 15 min, 4 °C). The resulting pellets were resuspended in Laemmli sample buffer, and proteins were resolved with 6% SDS-PAGE. To trap P-gp in the nucleotide-bound state the samples were preincubated in the presence of AMP-PNP (2 mM) for 20 min before the addition of fluorophore (13). Vanadate trapping was achieved by preincubation of the protein with 2 mM ATP and 300 μM sodium orthovanadate at 37 °C for 30 min before probe addition (13).

A further sample of denatured P-gp (*i.e.* fully accessible cysteine residues) was included in each assay to determine the signal produced by 100% labeling. The sample was subjected to ultracentrifugation as described above and resuspended in 2% (w/v) SDS to denature the protein and then incubated in the presence of probe (10 μM) for a further 3 h.

Analysis of P-gp Labeling with Cysteine-reactive Fluorescent Probes—Gels from the labeling reactions described above were analyzed using the BioDocIt Imaging system (UVP), which comprised a UV light source (λ = 302 nm) and a CCD camera. Images of the gels were quantified using densitometric analysis (NIH Image Software). Fluorescence intensity of the P-gp bands were expressed as a percentage of the denatured sample and plotted as a function of labeling time. The profiles were fitted using non-linear regression of the exponential association curve,

$$L = L_{max} \times (1 - e^{-kt}) \quad \text{(Eq. 2)}$$

where L is the percent labeled, L_{max} is the maximum percent labeled, t is time (min), and k is the observed rate constant for labeling.

The labeling rate constant may be converted to a half-life by the relationship $t_{½} = \text{Ln}2/k$. After imaging, the gels were stained with Coomassie Blue for 30 min as described above to ensure equivalent protein loading.

Data Analysis—All non-linear regression analyses were produced using the GraphPad Prism3.0 program. A minimum data set was obtained from at least three independent protein purification preparations, and all values are given as the mean ± S.E. Multiple data comparisons (>3 sets) were analyzed using ANOVA with a Newman-Keul post-hoc test, and statistical significance was presumed where $p < 0.05$.

RESULTS

Introduction of Single Cysteines into TM6 of P-gp Has Little Effect on the ATPase Activity—Expression levels for the various P-gp isoforms were similar (data not shown), and the yield of purified protein from 50 mg of crude membrane was in the range 41 ± 4 μg (S337C) to 65 ± 9 μg (Cys-less). Only the F335C isoform was consistently outside this range ($p < 0.05$, $n > 10$) and exhibited a yield of 28 ± 6 μg of P-gp. Reconstitution efficiencies were typically 95% of the protein co-migrating through sucrose gradients with 80% of the total lipid. Those samples where less than 70% of the protein co-migrated with less than 70% of total lipid displayed low ATPase activity and were excluded from further analysis.

The basal ATPase activity of Cys-less P-gp displayed a maximal activity (V_{max}) of 0.58 ± 0.15 μmol of P_i min^{-1} mg^{-1} characterized by an ATP affinity (K_m) of 0.58 ± 0.06 mM (Table I). In the presence of the non-transported P-gp modulator nicardipine, the activity was stimulated 2.9 ± 0.3-fold to a V_{max} = 1.46 μmol of P_i min^{-1} mg^{-1}. In contrast, the K_m for ATP was only marginally reduced to 0.38 ± 0.04 mM. The maximal unstimulated ATPase activities of the mutant P-gp isoforms containing a single cysteine in TM6 were in the range 0.35–0.65 μmol of P_i min^{-1} mg^{-1}, none of which was significantly different to that observed for Cys-less protein (Table I). Similarly, the K_m values (0.40–0.53 mM) did not differ statistically between the TM6 mutant isoforms, indicating that the catalytic cycle remained intact. Despite the introduction of mutations at positions throughout TM6, both the maximal ATPase activity (1.12–1.67 μmol of P_i min^{-1} mg^{-1}) and the degree of stimulation (2.2–3.5-fold basal) in the presence of nicardipine were not statistically different from the values observed for Cys-less P-gp (Table I). This indicates that the communication from the nicardipine binding site to the NBDs was unaffected by any of the changes introduced into TM6.

The effect of nicardipine on V_{max} and K_m was measured at a high concentration (30 μM) and may, therefore, mask subtle changes in potency caused by mutation of TM6 residues to cysteine. However, as shown in Table II, the potency for nicardipine to stimulate ATP hydrolysis did not vary significantly between the various isoforms (EC_{50} = 2.1–3.9 μM). This confirms that the nicardipine-P-gp interaction is unaffected by the mutations introduced into TM6. It has been previously demonstrated that P-gp contains at least four distinct drug binding sites (4) within the TMD. To examine the possibility that the introduced mutations generate differential effects on the drug binding sites, the interaction between vinblastine and P-gp was also characterized. Neither the degree to which ATP hydrolysis was stimulated by vinblastine (2.1–2.4-fold basal) nor the potency to stimulate ATPase activity (EC_{50} = 4.0–7.2 μM) for the TM6 mutations varied significantly. The results demonstrate that mutations introduced into TM6 did not alter the communication between the nicardipine and vinblastine binding sites with the NBDs. Moreover, they suggest that the binding event itself was unaffected.

Considerations for Labeling of Engineered Cysteine Residues—The introduction of cysteine residues at specific positions within TM6 produced P-gp isoforms essentially identical to the Cys-less template. Therefore, the relative abilities of the residues to react with three fluorescent probes displaying distinct physicochemical properties was employed as a means of "topographical mapping" for TM6. The probes used were FM, CM, and BM, which are shown in Fig. 1*a* and are known to

TABLE II
Potency of drugs that affect the ATPase activity of purified reconstituted single cysteine mutants of P-gp

Pure, reconstituted P-gp (0.3 μg) was incubated in the presence of ATP (2 mM) and varying concentrations of nicardipine, vinblastine, or vanadate. Hydrolysis of nucleotide was detected by the liberation of inorganic phosphate using a colorimetric assay. The potencies to stimulate (EC_{50}) or inhibit (IC_{50}) activity were derived from non-linear regression of the general dose-response relationship. Values refer to the mean ± S.E. obtained from a minimum of three independent protein purification preparations.

P-gp isoform	Potency of drug effect		
	Nicardipine, EC_{50}	Vinblastine, EC_{50}	Vanadate, IC_{50}
	μM	μM	μM
Cys-less	3.2 ± 0.3	4.2 ± 0.6	4.0 ± 0.4
V331C	3.3 ± 0.4	7.2 ± 1.7	3.2 ± 0.4
T333C	2.3 ± 0.2	4.6 ± 0.4	3.9 ± 0.8
F335C	2.3 ± 0.4	4.2 ± 0.8	5.5 ± 1.1
S337C	2.7 ± 0.5	4.1 ± 1.0	5.8 ± 0.8
L339C	2.1 ± 0.3	5.1 ± 0.8	4.2 ± 0.7
G341C	3.9 ± 0.5	4.0 ± 0.6	6.8 ± 1.3
F343C	2.1 ± 0.3	5.6 ± 2.7	2.7 ± 0.8

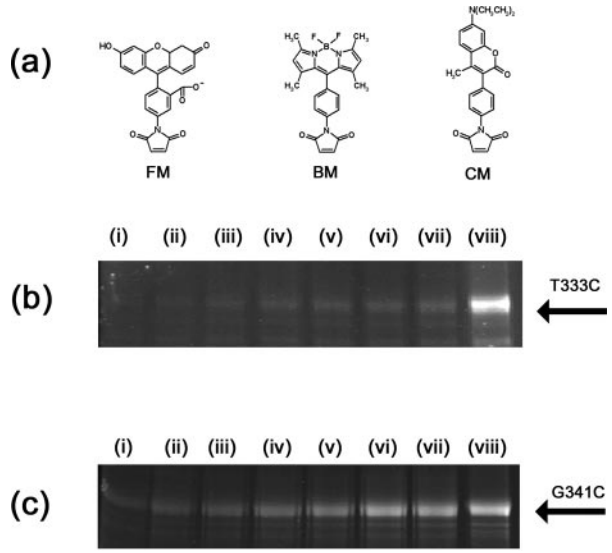

FIG. 1. **Labeling of single cysteine isoforms of P-gp with fluorescent maleimide reagents.** Structures of maleimide-containing probes (*a*) and the fluorescence profiles of SDS-PAGE gels obtained for time courses of fluorescein maleimide labeling of T333C (*b*) and coumarin maleimide labeling of G341C (*c*). *Lanes i-vii* refer to 10, 20, 30, 60, 120, 180, and 300 min of labeling. *Lane viii* demonstrates the fluorescence obtained in denatured P-gp isoforms. The amount of denatured sample loaded in gel (*panel b*) was equivalent to half that in the native samples and, therefore, refers to 50% of maximal labeling. In gel (*panel c*) the amount of denatured sample loaded was equivalent to native samples.

generate stable covalent bonds with thiol groups under physiological conditions. FM readily partitioned into the aqueous phase, with only 3% of the compound found in octanol (*i.e.* log P = −1.7 ± 0.2, n = 3). In contrast, CM and BM were considerably more hydrophobic, with partition extents of 95% (log P = 1.41 ± 0.1, n = 3) and 93% (log P = 1.1 ± 0.1, n = 3), respectively. Molecular modeling (DS Viewer Pro) indicated that although the probes have similar molecular volumes (FM = 287 Å^3, CM = 293 Å^3, BM = 291 Å^3), their topographies were markedly distinct. FM has a charged carboxyl group, thereby generating a hydrophilic face. CM has no charge, is relatively compact, and due to its hydrophobicity will likely partition into the bilayer in a random fashion. BM is bulky overall, has a delocalized positive charge, and is therefore likely to partition into the bilayer in a more ordered orientation compared with CM.

Because of the difficulty in removing unbound probes, a conventional fluorescence spectrophotometric assay could not be used to measure probe attachment to the single cysteine isoforms. The high partition coefficients of BM and CM rendered dialysis, ultrafiltration, and ultracentrifugation largely ineffective. Consequently a fluorescent SDS-PAGE method was adopted to separate labeled protein from unbound probe and enable quantitative analysis. Care was exercised to ensure that (i) band fluorescent intensities were within the linear range and (ii) that minor contaminating, cysteine-rich proteins do not interfere with analyses. Typical time courses for labeling of T333C with FM and G341C with CM are shown in Fig 1, *b* and *c*, respectively. *Panel b* shows a time-dependent increase in the labeling of T333C P-gp (*lanes i–vii*). *Lane viii* was loaded with half the amount of protein in *lanes i–vii*. The protein sample in *lane viii* had been denatured and, thus, provides a measure of 50% maximal attainable labeling. Quantification of *lanes i–vii* by comparison with *lane viii* shows that the level of labeling intensity was minimal (*i.e.* 6% at 300 min). All time courses for labeling with probes were normalized to denatured protein using this comparative approach. *Panel c* clearly demonstrates that the labeling of G341C reached significantly higher levels (*lanes i-vii*) when compared with denatured protein (*lane viii*), which in this case indicates 100% labeling.

Extents and Rates of Labeling of Residues in TM6 under Basal Conditions—Time courses similar to those shown in Fig. 1 were undertaken for all mutant P-gp isoforms and fitted with the exponential association equation to generate a maximal labeling intensity and the rate of this labeling reaction. Mutant G324C, which contains a cysteine in an accessible extracellular loop, was used as a positive control for labeling. Cys-less P-gp was used as a negative control, and labeling to specific isoforms was only deemed significant if it was significantly different to residual labeling observed for Cys-less protein. Figs. 2*a*, 3*a*, and 4*a* show the maximal extent of labeling obtained with the three probes to each isoform. Nonspecific labeling of Cys-less P-gp by FM was 4 ± 1% (Fig. 2*a*), whereas G324C labeled to 100% with a half-life of 12 ± 1 min (data not shown). Isoforms V331C, T333C, F335C, S337C, L339C, and G341C displayed labeling extents in the range 7–12%, and none was significantly different from the Cys-less isoform (ANOVA). In contrast, F343C in the native protein conformation was accessible to labeling with FM as adjudged by the 81 ± 2% labeling extent (L_{ext}), which was characterized by a half-life ($t_{½}$ = 47 ± 8 min) almost 4 times slower than observed for G324C. The data suggest that of the seven mutated residues in TM6, only Cys-343 was accessible to the hydrophilic probe FM.

The accessibilities of mutated TM6 residues to the hydrophobic probe CM (Fig. 3*a*) were considerably different to those obtained with FM. The level of nonspecific interaction with the Cys-less P-gp was higher (L_{ext} = 25 ± 4%), and G324C was also labeled by CM (L_{ext} = 102 ± 4%), although the half-life ($t_{½}$ = 31 ± 4 min) was almost 3 times slower than observed for FM. Each of the TM6 isoforms was fully labeled with CM as demonstrated by L_{ext} values in the range 87–107% (Fig. 3*a*), with similar half-lives in the range 35–52 min. Only the L339C isoform was significantly different with more rapid reaction kinetics ($t_{½}$ = 23 ± 1 min, $p < 0.05$, n = 3).

Labeling of mutant TM6 isoforms with BM generated a profile intermediate between those obtained with CM and FM (Fig. 4*a*), perhaps reflective of its distinct physicochemical properties. Nonspecific interaction with Cys-less protein was 19 ± 1% and G324C labeled fully (L_{ext} = 97 ± 3%) with a half-life approximately double ($t_{½}$ = 23 ± 2 min) that obtained for FM. Isoforms T333C, F335C, S337C, and G341C did not label with BM since the L_{ext} values (19–27%) were not signif-

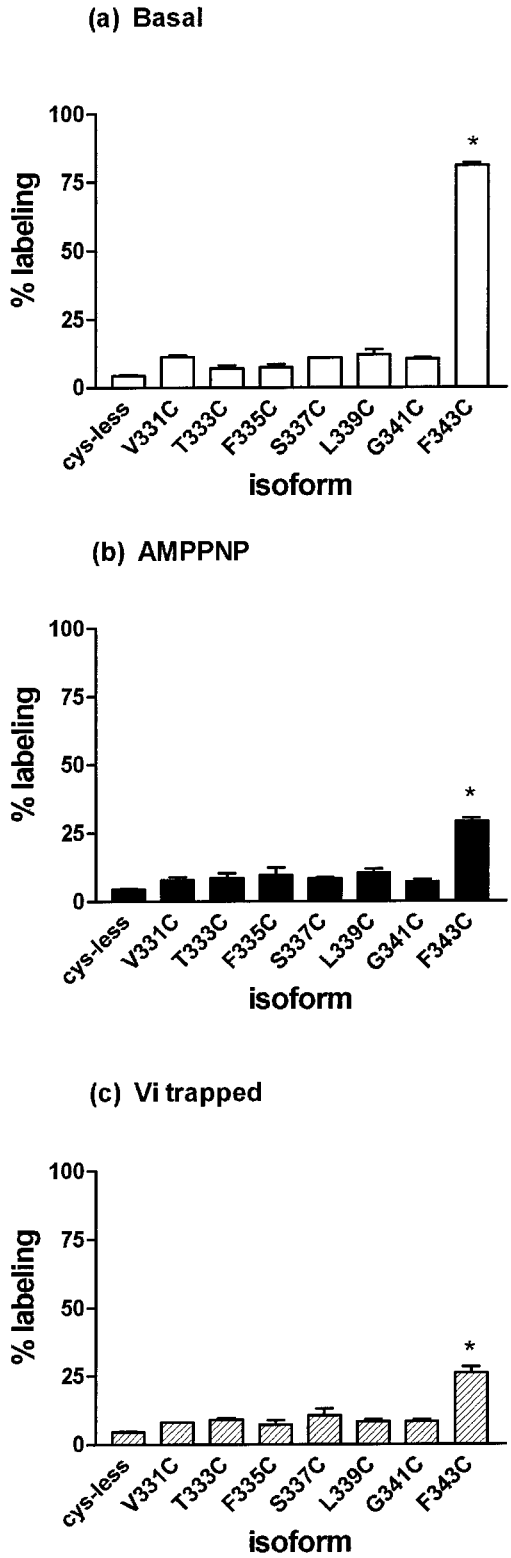

FIG. 2. **Extents of labeling mutant P-gp isoforms with fluorescein maleimide at different stages of the catalytic cycle.** Purified, reconstituted P-gp (1.5–3 μg) was labeled with fluorescein maleimide (10 μM) for 0–300 min. Labeling was determined by fluorescent imaging of SDS-PAGE gels and quantified with densitometry. The extent of labeling (*i.e.* % labeling) was expressed as a percentage of that obtained with denatured sample. Data were fitted with the exponential association curve using non-linear regression. Cys-less represents the cysteine-free mutant isoform. Labeling was undertaken for protein in the basal (*a*), AMP-PNP-bound (*b*), or ADP/vanadate-trapped (*c*) states of P-gp. The *asterisk* (*) indicates that labeling was significantly greater than the nonspecific fluorescence obtained with Cys-less P-gp ($p < 0.01$, ANOVA with Newman Kuel post hoc test).

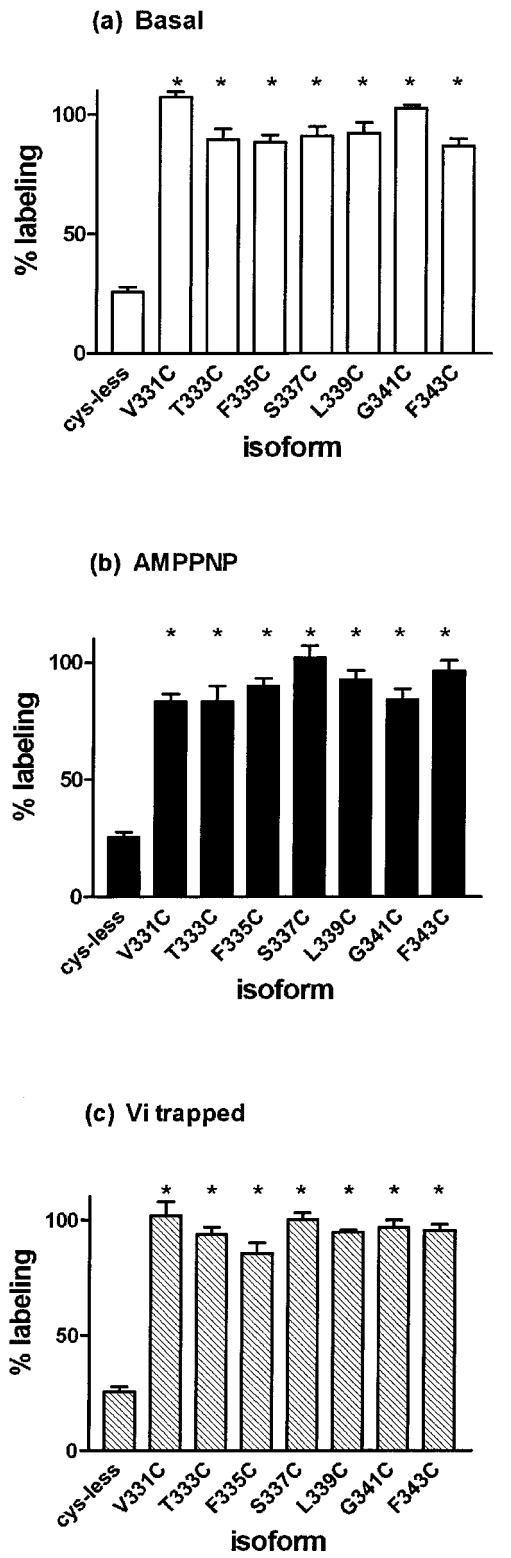

FIG. 3. **Extents of labeling mutant P-gp isoforms with coumarin maleimide at different stages of the catalytic cycle.** Purified, reconstituted P-gp (1.5–3 μg) was labeled with coumarin maleimide (10 μM) for 0–300 min. Labeling was determined by fluorescent imaging of SDS-PAGE gels and quantified with densitometry. The extent of labeling (*i.e.* % labeling) was expressed as a percentage of that obtained with denatured sample. Data were fitted with the exponential association curve using non-linear regression. Cys-less represents the cysteine-free mutant isoform. Labeling was undertaken for protein in the basal (*a*), AMP-PNP-bound (*b*), or ADP/vanadate-trapped (*c*) states of P-gp. The *asterisk* (*) indicates that labeling was significantly greater than the nonspecific fluorescence obtained with Cys-less P-gp ($p < 0.01$, ANOVA with Newman Kuel post hoc test).

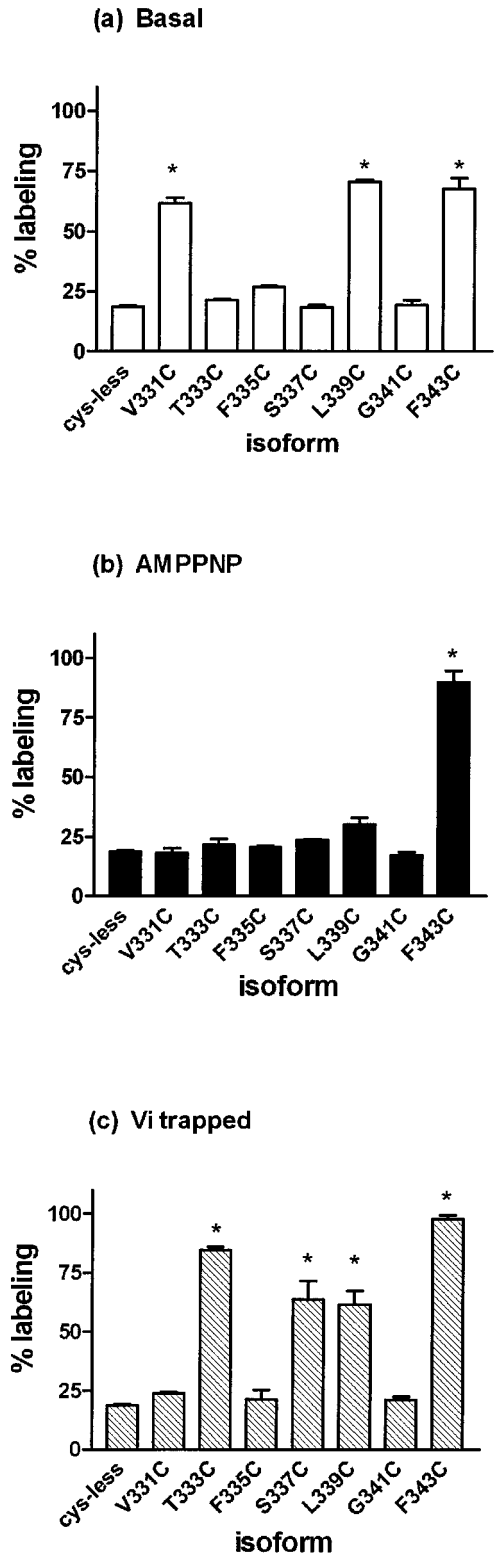

FIG. 4. **Extents of labeling mutant P-gp isoforms with BODIPY-maleimide at different stages of the catalytic cycle.** Purified, reconstituted P-gp (1.5–3 μg) was labeled with BODIPY-maleimide (10 μM) for 0–300 min. Labeling was determined by fluorescent imaging of SDS-PAGE gels and quantified with densitometry. The extent of labeling (*i.e.* % labeling) was expressed as a percentage of that obtained with denatured sample. Data were fitted with the exponential association curve using non-linear regression. Cys-less represents the cysteine-free mutant isoform. Labeling was undertaken for protein in the basal (*a*), AMP-PNP-bound (*b*), or ADP/vanadate-trapped (*c*) states of P-gp. The *asterisk* (*) indicates that labeling was significantly greater than the nonspecific fluorescence obtained with Cys-less P-gp ($p < 0.01$, ANOVA with Newman Kuel post hoc test).

icantly different from those observed with Cys-less P-gp. The V331C isoform was labeled with BM (L_{ext} = 62 ± 4%), although the half-life for this labeling was considerably slower ($t_{½}$ = 143 ± 21 min, $p < 0.05$) than obtained for any other reaction. L339C was also efficiently labeled with BM (L_{ext} = 71 ± 2%); however, the reaction kinetics were faster ($t_{½}$ = 49 ± 7 min) than observed with V331C. Surprisingly, mutant F343C, which was the only isoform labeled by the hydrophilic compound FM, reacted with the amphiphilic probe BM (L_{ext} = 68 ± 11%) with a half-life of only 18 ± 4 min.

Alterations in Labeling during the Catalytic Cycle—As discussed earlier, the ATP catalytic cycle is capable of inducing large conformational changes in the TMDs of P-gp. To determine whether TM6 is influenced by this stimulus, the accessibility of residues was determined in protein trapped at various stages of the catalytic cycle. AMP-PNP binding and vanadate trapping of P-gp were used to mimic the pre- and post-hydrolytic conformations (45). The maximal extents of labeling obtained from full time-course data are shown for each isoform to each probe in the presence of AMP-PNP (Fig. 2*b*, 3*b*, and 4*b*) or after vanadate trapping (Fig. 2*c*, 3*c*, and 4*c*). Isoform F343C was the only protein to label with the hydrophilic probe FM, and the labeling was significantly reduced by both AMP-PNP binding (L_{ext} = 29 ± 3%) and vanadate trapping (L_{ext} = 26 ± 4%). Despite the reduced extent of labeling, the values remained significantly different ($p < 0.05$) from those obtained with Cys-less P-gp (L_{ext} = 4 ± 1%). The residual labeled protein is likely to arise from the proportion of F343C P-gp that was not completely bound with AMP-PNP or vanadate-trapped. This was confirmed by similar labeling half-lives compared with nucleotide free F343C P-gp. F343C was the only isoform whose labeling with FM was affected by the catalytic cycle because all other mutant P-gp proteins remained inaccessible to labeling with this hydrophilic molecule.

AMP-PNP binding did not significantly affect the labeling of mutant TM6 isoforms by CM as evident by the L_{ext} values in the range 83–107% (Fig. 3*b*). Similarly, the kinetics of the reaction were also unchanged ($t_{½}$ values of 45–65 min) with the exception of isoform L339C. This protein was the most rapidly labeled with CM in the basal state ($t_{½}$ = 21 ± 1 min), and after AMP-PNP binding the half-life was increased to 45 ± 2 min. However, the most dramatic effects on CM labeling were observed in the vanadate-trapped protein. The extents of labeling remained similar, with all residues displaying high accessibility (L_{ext} > 85%) as shown in Fig. 3*c*. However the half-lives describing the labeling reaction were altered. Isoforms T333C ($t_{½}$ = 16 ± 3 min) and F343C ($t_{½}$ = 18 ± 5 min) labeled with CM with significantly increased rates compared with the values observed in either basal conditions or in the presence of AMP-PNP, reflecting an increased accessibility of the introduced cysteine residues. In the vanadate-trapped state, L339C labeling ($t_{½}$ = 28 ± 3 min) regained the rapid reaction kinetics with CM that were observed in the basal state but lost in the nucleotide-bound protein.

The extent to which the amphiphilic probe BM labeled the mutant P-gp isoforms Cys-331 and Cys-339 was greatly reduced in the AMP-PNP-bound state. Whereas under basal conditions V331C, L339C, and F343C were accessible to BM, only the latter was labeled (L_{ext} = 90 ± 8%) after AMP-PNP binding to the protein (Fig. 4*b*). This reflects a general reduction in the overall residue accessibility after AMP-PNP binding at positions other than Cys-343. This was further confirmed by the observation that the half-life of labeling with BM in F343C was unaffected by the binding of AMP-PNP ($t_{½}$ = 18 ± 1 min) compared with the basal state. Vanadate trapping of the F343C isoform also failed to alter either the extent (L_{ext} = 98 ± 3%) or

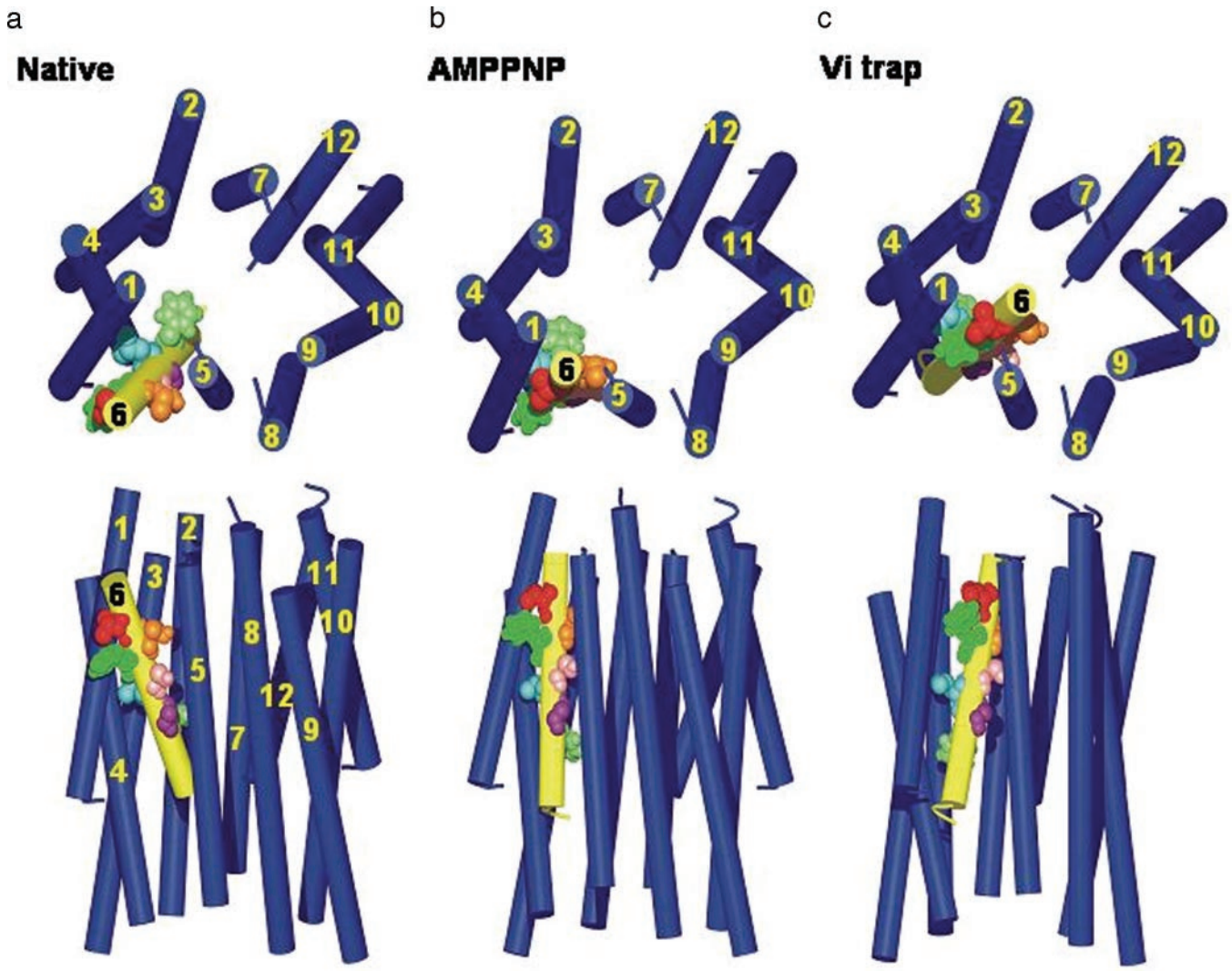

FIG. 5. **Proposed arrangements of transmembrane segments of P-gp at various stages of the catalytic cycle.** *a*, relative arrangements of transmembrane segments of P-gp based on the proposed atomic scale homology model (30). The NBDs and connecting loops have been removed, and the TM6 backbone is shown in *yellow*, whereas residues mutated to cysteine are also shown. The *upper panel* depicts the view from the extracellular face, and the *lower panel* shows a "side-on" view. *b*, TM6 has been tilted with respect to the long axis to describe the accessibility changes produced after the binding of AMP-PNP. *c*, TM6 has been tilted further to describe the accessibility changes produced after the transition from AMP-PNP-bound (pre-hydrolytic) to the ADP/vanadate-trapped (post-hydrolytic) (*Vi*) states.

half-life ($t_{½}$ = 14 ± 3 min) of labeling with BM (Fig. 4*c*). Thus, in the basal state this residue is accessible to the hydrophilic probe, and after progression through the catalytic cycle its labeling "switches" to a preference for more hydrophobic probes.

Isoform T333C, which was inaccessible to BM under basal conditions, remained so after nucleotide binding and only labeled to a significant extent in the vanadate-trapped state (L_{ext} = 85 ± 2%). In contrast, V331C was affected in the opposite manner with accessibility only apparent in the basal state. Residue Cys-337 only produced a significant level of labeling (L_{ext} = 64 ± 13%) when trapped in a post-hydrolytic state with ADP and vanadate (Fig. 4*c*). The effects on L339C accessibility to BM paralleled the observations with CM. Labeling with BM was observed in the basal state (L_{ext} = 71 ± 2%), lost in the nucleotide-bound state, and then recovered after ATP hydrolysis (L_{ext} = 62 ± 12%). Two isoforms, F335C and G341C, could not be labeled by BM under any conditions and presumably lie in a region with low accessibility due to proximity of other structural elements.

Overall, the results suggest that binding of AMP-PNP produces a conformational transition that decreases the accessibility of a substantial proportion of TM6 and reduces access to the aqueous environment. The subsequent hydrolytic step leads to formation of a third transition state that despite increases in accessibility of several TM6 residues to amphiphilic probes appears not to allow the introduced cysteines exposure to the aqueous environment.

DISCUSSION

TM6 has been widely implicated in mediating a key role in drug transport by P-gp, although the exact molecular pathway(s) or mechanism remains unknown. If TM6 is important then it is likely to be involved in the bi-directional communication between the TMDs and NBDs of P-gp that is essential for a coupled transport process. The present investigation supports this hypothesis by demonstrating that the topography of TM6 undergoes significant reconfiguration between the nucleotide-free, the nucleotide-bound, and post-hydrolytic states of P-gp. The topographical information and its nucleotide-driven changes have been related to an atomic scale molecular model recently presented for the nucleotide free state of P-gp (30).

Fig. 5*a* provides the relative arrangements of the 12 TM segments in P-gp under basal conditions based on the model for

nucleotide-free P-gp and excludes connecting loops and NBDs for clarity (30). The relative arrangement of TMs 5, 6, 11, and 12 around a central pore within the model agrees with the majority of available cross-linking data for P-gp (25, 26, 46). The side view of the region near TM6 indicates that a large number of the residues mutated appear to face the lipid environment, which accounts for the ease of labeling obtained with CM throughout. The low accessibility of residues Cys-333, Cys-337, and Cys-341 to labeling with BM, which is "bulkier" than CM, is due to their location at the interface between TM5 and TM6. Of particular relevance is the protrusion of Cys-343 into the central aqueous cavity, thereby rendering it susceptible to labeling with the hydrophilic probe FM. Although residue Cys-339 also displays some access to the central cavity, its close proximity to TM1 provides a barrier to labeling with the "bulkiest" probe, FM. Residues Cys-331 and Cys-335 face the lipid milieu and are, therefore, readily labeled by CM; however, only the former is accessible to BM, and the time course for the interaction is quite slow. Conceivably, residues proximal to Cys-331 and Cys-335 provide a barrier to BM. Overall, the topography of TM6 of the model is in good agreement with the data presented in the current investigation, and the model was subsequently used to infer the structural changes accompanying nucleotide binding.

One of the initial events in the transport process is nucleotide binding, but how important is this event to the overall drug translocation mechanism? Evidence from investigations of cross-link formation between helices surrounding the central cavity (*i.e.* TMs 5, 6, 11, and 12) suggest that ATP binding does not lead to significant structural change (28, 47). However, structural information using either electron microscopy (21, 22) or spectroscopy-based approaches (19, 20) indicates the contrary. These structural investigations are supported by a wealth of functional information demonstrating a key role for binding of nucleotide to instigate the translocation process (13, 18, 45, 48, 49). A drawback with the cross-linking studies mentioned above is the necessity for large conformational changes to enable detection and a reliance on the cross-link to affect protein migration in SDS-PAGE. In addition, the studies did not provide kinetic data on the interactions nor did they involve full dose-response analyses, and together there is potential to overlook more subtle conformational changes. In the present investigation binding of the non-hydrolyzable ATP analogue, AMP-PNP, produced a general loss in residue accessibility that was most apparent for Cys-331 and Cys-339 and the removal of Cys-343 from an aqueous accessible environment. The possible structural changes to explain these changes include TM rotation, translational movement, or tilting. Fig. 5, *b* and *c*, present proposed schematic models of P-gp TMDs that best reflect the fluorescence labeling data described and producing the most parsimonious alterations to TM6.

Although anti-clockwise rotation of TM6 would explain the loss of Cys-339 and Cys-343 accessibility through their closer approach to TM1, it does not explain the loss of Cys-331 labeling by BM and would suggest that Cys-333 movement away from TM5 would render it susceptible to labeling. Conversely, clockwise rotation of TM6 would account for the reduced Cys-331 and Cys-343 labeling since the former would approach TM1, and the latter moves closer to TM5. However, residue Cys-339 would protrude directly into the central cavity and thereby gain accessibility to FM, which it clearly does not. Similarly, lateral movement of TM6 either to TM5 or to the vicinity of TM1/TM4 can only explain a part of the data. In contrast tilting or "straightening" of the longitudinal axis of TM6 provides a more complete description. Tilting of TM6 would bring Cys-331 and Cys-335 closer to TM1 and account for their low accessibility, whereas Cys-333, Cys-337, and Cys-341 remain packed against TM5. Residue Cys-339 is brought into the proximity of TM1/TM4, hence its lower accessibility, and Cys-343 assumes a configuration similar to Cys-339 in the native state. Both the atomic model (30) and cross-linking data (50) suggest that TM6 and TM12 are close to the cytoplasmic leaflet of the bilayer, and it has been argued that this interaction is used to "block" the aqueous cavity. Consequently, if TM6 were to tilt in response to ATP binding the effect would extend the depth of the central cavity in P-gp, a finding that is supported by structural investigations (22).

The next stage of drug transport is driven by the hydrolysis of nucleotide and data from EM, and spectroscopy-based investigations suggest that P-gp assumes a conformation that is distinct from both the native and nucleotide-bound forms (19–22). The present characterization of residue accessibility to thiol-reactive probes concurs with a third distinct conformation. The major topographical changes in moving from the AMP-PNP- to the ADP.Vi-bound state was accessibility of residues Cys-333 and Cys-337 in addition to regaining Cys-339 labeling with BM. Cross-linking investigations with Tris-(2-maleimidoethyl)amine suggest that TM6 rotates in an anti-clockwise fashion (51). A more recent study by the same authors provides an alternative conformational change in response to ATP hydrolysis, namely that TM segments at the extracellular face are brought closer together (47), analogous to a tilting movement. Rotational changes only account for a part of the current accessibility data; however, tilting of TM6 such that the "extracellular" region is brought into the central cavity provides a more complete reconciliation. Further tilting of TM6 would relieve the obstruction of Cys-339 to labeling caused by TM1 in the nucleotide-bound state. Furthermore, Cys-331 and Cys-335 would remain close to TM1 and, thus, inaccessible to labeling. Residues Cys-333 and Cys-337 move away from TM5 and become labeled by BM and, since the former is furthest from TM5, provides an explanation for its more rapid reaction with the probe. Cys-341 remains close to TM5 and is only labeled with CM, whereas Cys-343 remains localized as in the AMP-PNP-bound state and, thus, inaccessible to FM.

The tilting of TM6 thereby provides a consistent explanation for the data presented in the current investigation but also for previous studies using cysteine-scanning mutagenesis and covalent cross-link formation. The EM data suggest that TM6 is unlikely to be the only segment to undergo conformational changes. Our data analysis predicts the tilting of TM6 relative to those in proximity, but this does not rule out movement of other helices. The helical tilting hypothesis also provides a mechanism for interdomain communication during transport, particularly given that TM6 is directly joined to the N-terminal NBD. Finally, the nucleotide-driven tilting of TM6 is also compatible with the demonstrated alterations in drug binding site affinity during ATP catalysis (13).

Acknowledgment—The assistance of the JRLoF in lipid preparations was greatly appreciated.

REFERENCES

1. Shapiro, A. B., Fox, K., Lam, P., and Ling, V. (1999) *Eur. J. Biochem.* **259,** 841–850
2. Shapiro, A. B., and Ling, V. (1997) *Eur. J. Biochem.* **250,** 130–137
3. Tamai, I., and Safa, A. R. (1991) *J. Biol. Chem.* **266,** 16796–16800
4. Martin, C., Berridge, G., Higgins, C. F., Mistry, P., Charlton, P., and Callaghan, R. (2000) *Mol. Pharmacol.* **58,** 624–632
5. Greenberger, L. M., Lisanti, C. J., Silva, J. T., and Horwitz, S. B. (1991) *J. Biol. Chem.* **266,** 20744–20751
6. Bruggeman, E. P., Germann, U. A., Gottesman, M. M., and Pastan, I. (1989) *J. Biol. Chem.* **264,** 15483–15488
7. Dean, M., Hamon, Y., and Chimini, G. (2001) *J. Lipid Res.* **42,** 1007–1017
8. al-Shawi, M. K., and Senior, A. E. (1993) *J. Biol. Chem.* **268,** 4197–4206
9. Urbatsch, I. L., Sankaran, B., Bhagat, S., and Senior, A. E. (1995) *J. Biol. Chem.* **270,** 26956–26961
10. Urbatsch, I. L., Sankaran, B., Weber, J., and Senior, A. E. (1995) *J. Biol. Chem.*

270, 19383–19390
11. Tanford, C. (1983) *Annu. Rev. Biochem.* **52,** 379–409
12. Krupka, R. M. (1993) *Biochem. Biophys. Acta* **1183,** 114–122
13. Martin, C., Higgins, C. F., and Callaghan, R. (2001) *Biochemistry* **40,** 15733–15742
14. Sauna, Z. E., and Ambudkar, S. V. (2000) *Proc. Natl. Acad. Sci. U. S. A.* **97,** 2515–2520
15. Urbatsch, I. L., Al-Shawi, M. K., and Senior, A. E. (1994) *Biochemistry* **33,** 7069–7076
16. Sharom, F. J. (1995) *J. Bioenerg. Biomembr.* **27,** 15–22
17. Liu, R., and Sharom, F. J. (1996) *Biochemistry* **35,** 11865–11873
18. Druley, T. E., Stein, W. D., and Roninson, I. B. (2001) *Biochemistry* **40,** 4312–4322
19. Sonveaux, N., Vigano, C., Shapiro, A. B., Ling, V., and Ruysschaert, J. M. (1999) *J. Biol. Chem.* **274,** 17649–17654
20. Sonveaux, N., Shapiro, A. B., Goormaghtigh, E., Ling, V., and Ruysschaert, J. M. (1996) *J. Biol. Chem.* **271,** 24617–24624
21. Rosenberg, M. F., Velarde, G., Ford, R. C., Martin, C., Berridge, G., Kerr, I. D., Callaghan, R., Schmidlin, A., Wooding, C., Linton, K. J., and Higgins, C. F. (2001) *EMBO J.* **20,** 5615–5625
22. Rosenberg, M. F., Kamis, A. B., Callaghan, R., Higgins, C. F., and Ford, R. C. (2003) *J. Biol. Chem.* **278,** 8294–8299
23. Locher, K. P., Lee, A. T., and Rees, D. C. (2002) *Science* **296,** 1091–1098
24. Chang, G. (2003) *J. Mol. Biol.* **330,** 419–430
25. Loo, T. W., and Clarke, D. M. (2000) *J. Biol. Chem.* **275,** 5253–5256
26. Loo, T. W., Bartlett, M. C., and Clarke, D. M. (2004) *J. Biol. Chem.* **279,** 7692–7697
27. Loo, T. W., and Clarke, D. M. (1996) *J. Biol. Chem.* **271,** 27482–27487
28. Loo, T. W., and Clarke, D. M. (1997) *J. Biol. Chem.* **272,** 20986–20989
29. Loo, T. W., and Clarke, D. M. (2000) *J. Biol. Chem.* **275,** 39272–39278
30. Stenham, D. R., Campbell, J. D., Sansom, M. S., Higgins, C. F., Kerr, I. D., and Linton, K. J. (2003) *FASEB J.* **17,** 2287–2289
31. Bruggemann, E. P., Currier, S. J., Gottesman, M. M., and Pastan, I. (1992) *J. Biol. Chem.* **267,** 21020–21026
32. Greenberger, L. M. (1993) *J. Biol. Chem.* **268,** 11417–11425
33. Ecker, G. F., Csaszar, E., Kopp, S., Plagens, B., Holzer, W., Ernst, W., and Chiba, P. (2002) *Mol. Pharmacol.* **61,** 637–648
34. Glossmann, H., Ferry, D. R., Striessnig, J., Goll, A., and Moosburger, K. (1987) *Trends Pharmacol. Sci.* **8,** 95–100
35. Gros, P., Dhir, R., Croop, J., and Talbot, F. (1991) *Proc. Natl. Acad. Sci. U. S. A.* **88,** 7289–7293
36. Kajiji, S., Talbot, F., Grizzuti, K., Van Dyke-Phillips, V., Agresti, M., Safa, A. R., and Gros, P. (1993) *Biochemistry* **32,** 4185–4194
37. Hanna, M., Brault, M., Kwan, T., Kast, C., and Gros, P. (1996) *Biochemistry* **35,** 3625–3635
38. Hafkemeyer, P., Dey, S., Ambudkar, S. V., Hrycyna, C. A., Pastan, I., and Gottesman, M. M. (1998) *Biochemistry* **37,** 16400–16409
39. Devine, S. E., Ling, V., and Melera, P. W. (1992) *Proc. Natl. Acad. Sci. U. S. A.* **89,** 4564–4568
40. Chen, G., Duran, G. E., Steger, K. A., Lacayo, N. J., Jaffrezou, J. P., Dumontet, C., and Sikic, B. I. (1997) *J. Biol. Chem.* **272,** 5974–5982
41. Blott, E. J., Higgins, C. F., and Linton, K. J. (1999) *EMBO J.* **18,** 6800–6808
42. Taylor, A. M., Storm, J., Soceneantu, L., Linton, K. J., Gabriel, M., Martin, C., Woodhouse, J., Blott, E., Higgins, C. F., and Callaghan, R. (2001) *Br. J. Pharmacol.* **134,** 1609–1618
43. Gabriel, M. P., Storm, J., Taylor, A. M., Linton, K. J., Kerr, I. D., and Callaghan, R. (2003) *Biochemistry* **42,** 7780–7789
44. Chifflet, S., Chiesa, U. T. R., and Tolosa, S. (1988) *Anal. Biochem.* **168,** 1–4
45. Martin, C., Berridge, G., Mistry, P., Higgins, C., Charlton, P., and Callaghan, R. (2000) *Biochemistry* **39,** 11901–11906
46. Loo, T. W., and Clarke, D. M. (2001) *J. Biol. Chem.* **276,** 14972–14979
47. Loo, T. W., and Clarke, D. M. (2002) *Proc. Natl. Acad. Sci. U. S. A.* **99,** 3511–3516
48. Sauna, Z. E., and Ambudkar, S. V. (2001) *J. Biol. Chem.* **276,** 11653–11661
49. Julien, M., and Gros, P. (2000) *Biochemistry* **39,** 4559–4568
50. Loo, T. W., and Clarke, D. M. (2001) *J. Biol. Chem.* **276,** 36877–36880
51. Loo, T. W., and Clarke, D. M. (2001) *J. Biol. Chem.* **276,** 31800–31805

The Topography of Transmembrane Segment Six Is Altered during the Catalytic Cycle of P-glycoprotein

Alice Rothnie, Janet Storm, Jeff Campbell, Kenneth J. Linton, Ian D. Kerr and Richard Callaghan

J. Biol. Chem. 2004, 279:34913-34921.
doi: 10.1074/jbc.M405336200 originally published online June 10, 2004
